Available Online

J. Sci. Res. **16** (3), 899-915 (2024)

JOURNAL OF SCIENTIFIC RESEARCH

www.banglajol.info/index.php/JSR

Exploring the Anticorrosion Performance of 2-(((4-Chlorobenzyl) Thiol) Methyl)-1H-Benzo[d]imidazole on Aluminum in 1 M HNO_3

T. H. Rokia[1], M. A. Tigori[2,*], A. A. Koffi[1], P. M. Niamien[1]

[1]Laboratoire de Constitution et Réaction de la Matière, Unité de Formation et de Recherche des Sciences des Structures de la Matière et de Technologie, Université Félix Houphouët Boigny, Abidjan, Côte d'Ivoire

[2]Laboratoire des Sciences et Technologies de l'Environnement, Unité de Formation et de Recherche Environnement, Université Jean Lorougnon Guédé, Daloa, Côte d'Ivoire

Received 26 March 2024, accepted in final revised form 6 June 2024

Abstract

Organic corrosion inhibitors play a vital role in controlling and reducing corrosion. It is in this context that 2-(((4-chlorobenzyl) thiol) methyl)-1H-benzo[d]imidazole was inspected as an inhibitor of aluminum corrosion in HNO_3 medium. Gravimetric techniques and density functional theory (DFT) were conducted to prove the inhibition activity of this compound. Experimental results indicate that the inhibition potency of this compound increases with its concentration and decreases with increasing temperature. Indeed, the maximum inhibition efficiency reaches 97.74 % at concentration C_{inh}=5.10^{-3} M and at temperature T = 298 K. Adsorption isotherms study indicates that there is a strong interaction between the particles adsorbed on metal surface with adsorbed layer stability. The adsorption process is dominated by physical adsorption with increased disorder. Activated thermodynamic parameters were calculated and examined. Theoretical data derived from DFT calculations explained the adsorption process of the compound to metal surface. These theoretical data are consistent with the experimental results.

Keywords: 2-(((4-chlorobenzyl) thiol) methyl)-1H-benzo[d]imidazole; Aluminum corrosion; Gravimetric techniques; Density functional theory; Inhibition activity.

doi: https://dx.doi.org/10.3329/jsr.v16i3.72318 J. Sci. Res. **16** (3), 899-915 (2024)

1. Introduction

The use of synthetic molecules to mitigate metal corrosion has become an approved means of protection in many sectors [1]. Indeed, because of certain organic and inorganic molecules toxicity, constant efforts are being made to develop corrosion inhibitors with low toxicity and no harm to the environment [2-4]. Moreover, in a bid to better control this toxicity, several researchers have embarked on an approach to develop synthetic organic inhibitors [5-7]. These compounds need to be more environmentally friendly, or even closer to natural compounds, in order to combat metal corrosion without affecting users' health. Furthermore, it has been proven that, in addition to its minimal toxic effect on the

* *Corresponding author*: tigori20@yahoo.fr

environment, a good inhibitor must be easily accessible and low-cost [8,9]. This accessibility will enable all users to deal with corrosion phenomenon without great difficulty. Corrosion contributes to metals and alloys degradation, transforming them into more stable forms such as oxides and sulfides. The development of environmentally-friendly organic inhibitors containing heteroatoms such as N, S, P, O and aromatic rings would therefore be advantageous for controlling corrosion propagation in industrial environment [10-12]. The industrial sector uses acid solutions to maintain metal equipment. This operation deteriorates equipment and causes huge economic losses in corroded installations replacement [13,14]. The synthesized organic compounds can reduce aluminum corrosion rate, which is widely used because of its excellent properties. In addition, maintenance operations using acid solutions promote aluminum degradation. By combining synthetic compounds with these acid solutions, a stable covering film is formed on aluminum surface, isolating much metal from the aggressive environment. Most corrosion assessment methods do not provide detailed information on the interactions between metal and inhibitor. That's why in this work, density functional theory (DFT) based on quantum chemistry has been used to shed light on aluminum corrosion inhibition mechanism by 2-(((4-chlorobenzyl) thiol) methyl)-1H-benzo[d]imidazole [15,16]. This compound is a derivative of benzimidazole, which is used in various therapeutic products such as anti-ulcers, antihypertensive, antivirals, antifungals, anticancer and antihistamines [17]. It is a synthetic product that possesses heteroatoms (N,S) and π-bonds in its molecular structure that can ensure the various electronic transactions with the metal. Thus, the present work consists in studying the reaction of 2-(((4-chlorobenzyl) thiol) methyl)-1H-benzo[d]imidazole for aluminum inhibition in 1M HNO_3.

2. Experimental Part

2.1. *Chemicals*

Commercial nitric acid of 69 % purity, a concentration of 1 M was prepared from this commercial solution used as a blank for corrosion tests. A 99.5 % acetone was used to remove traces of grease and native oxide from aluminum samples. 2-(((4-chlorobenzyl) thiol) methyl)-1H-benzo[d]imidazole with molecular weight $C_{17}H_{16}N_2O_2S$ and molecular mass 312 g mol^{-1} was synthesized and characterized at Organic Chemistry and Natural Synthesis Laboratory of Felix Houphouët Boigny University. Using this molecule, eight concentrations were prepared which are: 0.001 mM, 0.005 mM, 0.01 mM, 0.05 mM, 0.1 mM, 0.5 mM, 1.0 mM and 5.0 mM. The chemical structure is presented in Fig. 1.

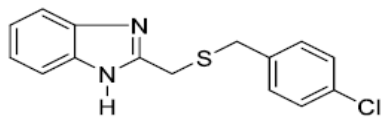

Fig. 1. Molecular structure 2-(((4-chlorobenzyl) thiol) methyl)-1H-benzo[d]imidazole (2-4-CBTM1HBI).

2.2. *Weight loss method*

Weight loss measurements consist in monitoring the evolution of an aluminum sample mass in HNO_3 solution with or without 2-4-CBTM1HBI. Cylindrical full aluminum samples 1 cm high and 0.25 cm in diameter were first sanded with abrasive paper of decreasing grain size from 40 to 600. They were then washed thoroughly with distilled water and degreased with acetone. They were dried in an oven at 80 °C and then weighed (m_1) with a precision analytical balance of ±0.0001 g. Each sample is immersed in 50 mL of 1 M HNO_3 with or without the different concentrations of 2-4-CBTM1HBI. After 1 h, the sample is removed from the solution and then rinsed extensively with distilled water. It is dried and then weighed again (m_2). Each test was repeated at 298 K, 308 K, 318 K, 328 K and 338 K. Aluminum corrosion rate was determined from this expression:

$$w = \frac{m_2 - m_1}{St} \quad (1)$$

Where, *S* is aluminum sample total surface and *t* is the immersion time.

2.3. *Computational modeling*

Theoretical calculations used in this work were carried out using Gaussian 03 software [18]. All the estimates around these calculations were performed in 6-311++G (d, p) basis with B3LYP functional (with the 3 exchanges of the Becke parameter: Lee, Yang, Parr) [19].The geometric optimization of the molecule (Fig. 2) was elaborated with the Gaussview application and in B3LYP/6-311++(d,p).The quantum chemical descriptors obtained were analyzed in detail.

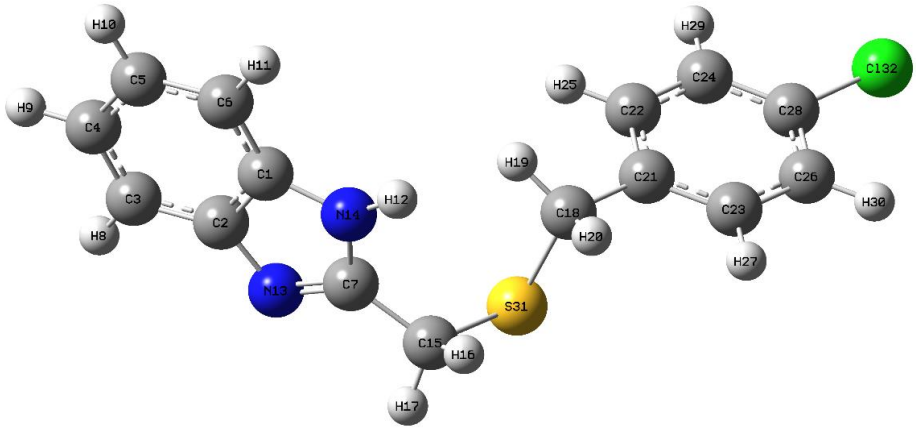

Fig. 2. Optimized structure 2-4-CBTM1HBI.

3. Results and Discussion

3.1. *Weight loss outcomes analysis*

3.1.1. *Temperature and 2-4-CBTM1HBI concentration influence on corrosion rate*

Temperature effect of aluminum corrosion rate in 1M HNO_3 solution is revealed by Fig. 3.

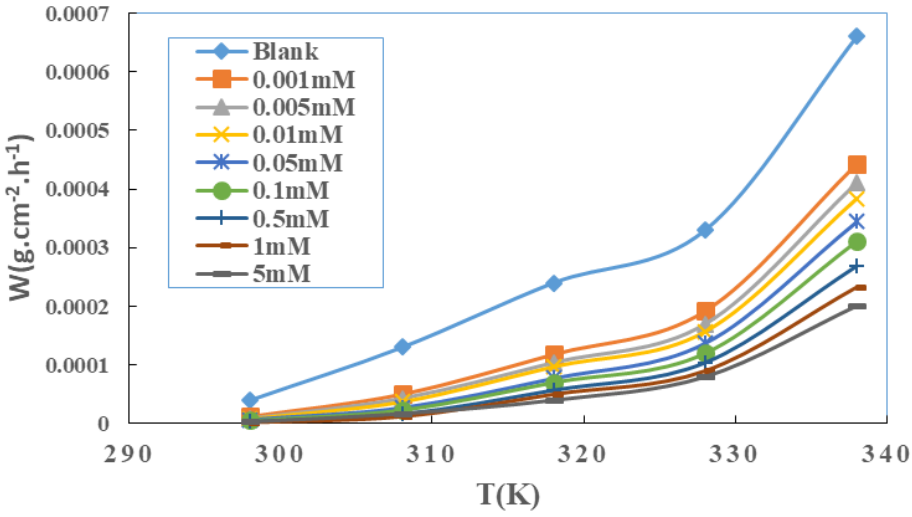

Fig. 3. Corrosion rate versus temperature.

These results state that aluminum corrosion rate increases with temperature. This corrosion rate evolves very rapidly in 2-4-CBTM1HBI absence. While in 2-4-CBTM1HBI presence, this corrosion rate decreases progressively with increasing inhibitor concentration. These results indicate that 2-4-CBTM1HBI presence in corrosive solution reduces electrons loss from aluminum. Moreover, as 2-4-CBTM1HBI concentration increases, the molecule is more accessible to supply electrons to the metal in replacing its lost electrons.

3.1.2. *Temperature and 2-4-CBTM1HBI concentration influence on inhibition efficiency*

Inhibition efficiency is determined by the following expression [20]:

$$IE(\%) = \frac{w_0 - w}{w_0} \times 100 \quad (2)$$

Where w_0 and w are respectively the corrosion rates in the absence and presence of 2-4-CBTM1HBI.

The evolution of inhibition efficiency as a function of temperature and inhibitor concentration is illustrated in Fig. 4.

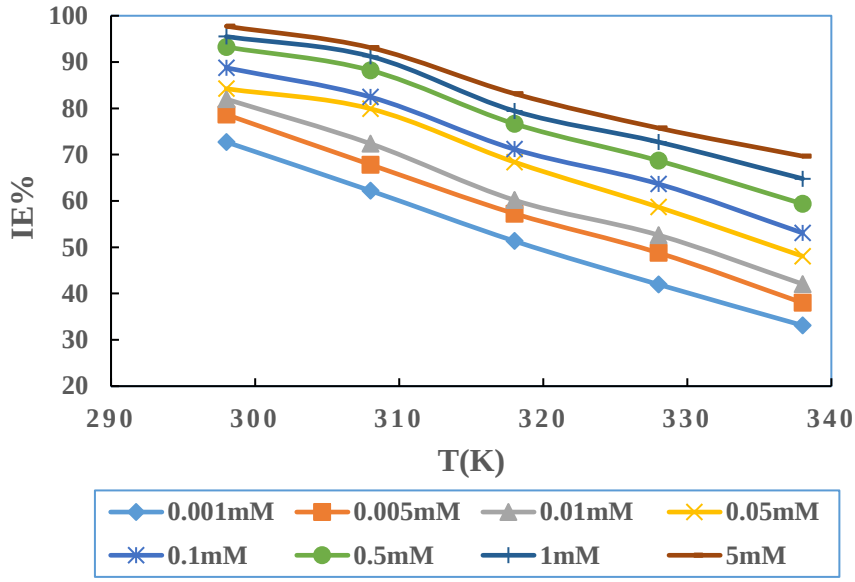

Fig. 4. Inhibition efficiency rate versus temperature

Fig. 4 reveals that the inhibition efficiency decreases as corrosive solution temperature increases. While inhibition efficiency increases as 2-4-CBTM1HBI concentration increases. These results indicate that the molecule adsorbs less and less on aluminum surface when the temperature increases and that this adsorption increases when the concentration of CBTM1HBI increases. It has been noted that the corrosion rate of aluminum increases with temperature, so aluminum increasingly loses its electrons as the temperature rises. Indeed, the corrosion of a metal is the loss of its electrons [21,22]. Thus, when this loss of electrons becomes high, the electrons supplied by the molecule are not sufficient to carry out the replacement, which justifies the drop in inhibition efficiency when the temperature evolves. CBTM1HBI highest inhibition efficiency is 97.74 at 298 K with C_{inh}=5.10^{-3} M and the lowest value is 33.33 at 338 K with C_{inh}=10^{-6}M concentration. Similar results have been reported in the literature [23,24].

3.1.2. *Suitable adsorption isotherm*

The adsorption model for an inhibitor is the relationship between the corrosion rate (θ) and its concentration (C_{inh}). The corrosion rate is expressed as follows [20]:

$$\theta = \frac{w_0 - w}{w_0} \quad (3)$$

To determine the most appropriate isotherm model, Langmuir, Temkin, El-Awady, Freundlich and Flory-Huggins isotherms have been tested. The Langmuir isotherm proved to be the most suitable adsorption model for characterizing CBTM1HBI adsorption nature

because the coefficients of determination for this isotherm are closest to unity. The expression of this isotherm is [25,26]:

$$\frac{C_{inh}}{\theta} = \frac{1}{K_{ads}} + C_{inh} \quad (4)$$

Experimental results applied to this model have permitted to represent this isotherm (Fig. 5). The parameters of the lines obtained are listed in the Table 1.

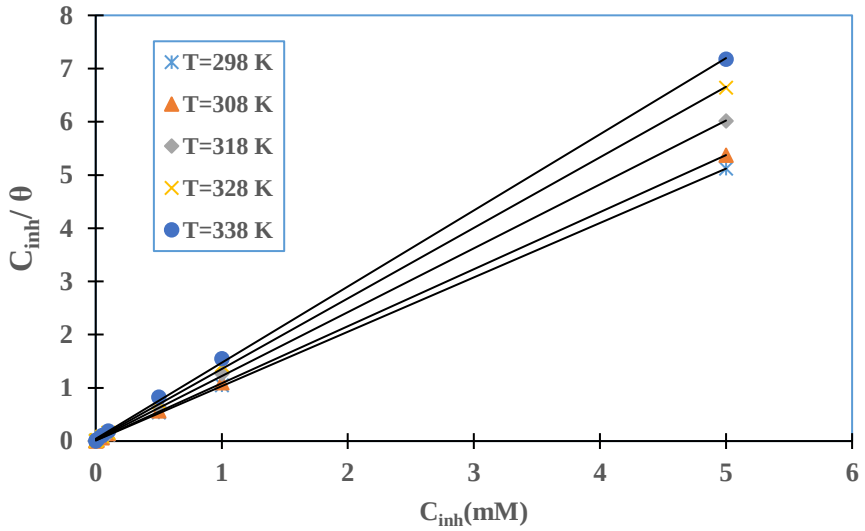

Fig. 5. $\frac{C_{inh}}{\theta}$ versus C_{inh}.

Table 1. Langmuir isotherm parameters.

T(K)	Equations	R^2	K_{ads}(M^{-1})
298	$\frac{C_{inh}}{\theta} = 1.0221C_{inh} + 0.0093$	1	107526.8817
308	$\frac{C_{inh}}{\theta} = 1.0718C_{inh} + 0.0143$	0.9999	69930.06993
318	$\frac{C_{inh}}{\theta} = 1.2005C_{inh} + 0.0202$	0.9999	49504.9505
328	$\frac{C_{inh}}{\theta} = 1.3259C_{inh} + 0.0289$	0.9998	34602.07612
338	$\frac{C_{inh}}{\theta} = 1.4305C_{inh} + 0.0420$	0.9997	23809.52381

Table 1 exploration indicates that the slopes of straight lines obtained are greater than 1. According to the model equation, the values of these slopes must be equal to 1. Thus, although the determination coefficients of this model are closest to unity, the adsorption of CBTM1HBI to aluminum surface does not strictly obey the model. In these circumstances, according to previous studies, the best-suited model is Villamil isotherm or the modified Langmuir isotherm. The equation for this isotherm is given by the following relationship [27]:

$$\frac{C_{inh}}{\theta} = \frac{n}{K_{ads}} + nC_{inh} \quad (5)$$

Where *n* expresses the slope of the straight lines. This adsorption type reveals that there is interaction between the adsorbed particles (inhibitor protonated form and NO_3^- ions) on metal surface and that each particle occupies more than one site [28]. These observations attest that the metal surface to which the inhibitor molecules attach is heterogeneous. Adsorption is multilayered, with the presence of interaction forces between adsorbed molecules. These different interactions indicate the existence of physical adsorption on aluminum surface.

3.1.3. *Thermodynamics of adsorption process*

Thermodynamic aspect of adsorption process is based of K_{ads} values determined from Villamil model. This aspect permit to give the properties of CBTM1HBI adsorption on aluminum surface. The thermodynamic adsorption parameters which are free adsorption enthalpy (ΔG^0_{ads}), standard adsorption enthalpy (ΔH^0_{ads}) and standard adsorption entropy (ΔS^0_{ads}) have been determined respectively from the following relationships [29]:

$$\Delta G^0_{ads} = -RTln(55.5K_{ads}) \quad (6)$$

$$\Delta G^0_{ads} = \Delta H^0_{ads} - T\Delta S^0_{ads} \quad (7)$$

Where *R* is Perfect gas constant; *T* is absolute temperature; 55.5 is the molar concentration of water in the solution. The representation of ΔG^0_{ads} as a function of temperature (Fig. 6) provides access to ΔH^0_{ads} and ΔS^0_{ads} values. These values are listed in Table 2.

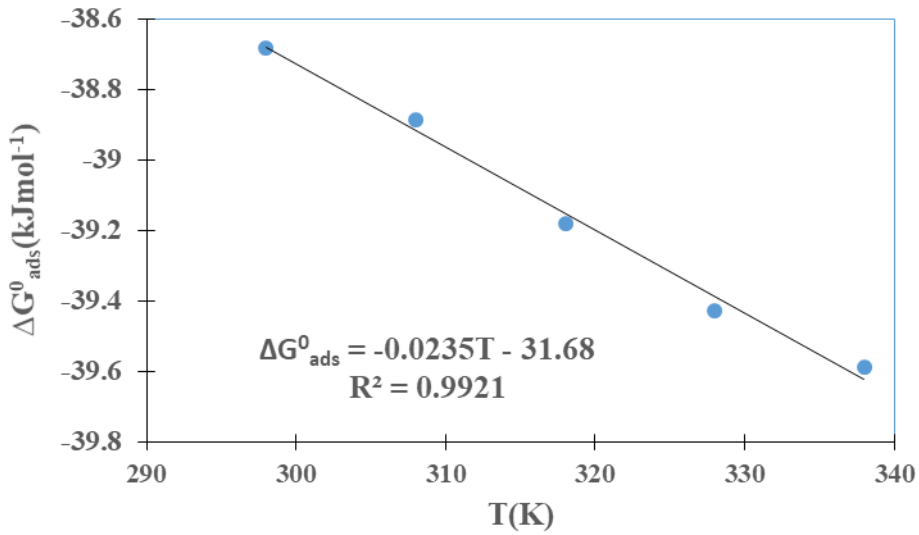

Fig. 6. ΔG^0_{ads} versus température.

Table 2. Valeurs de ΔG^0_{ads}, ΔH^0_{ads} et ΔS^0_{ads}

T(K)	$\Delta G^0_{ads}(kJ\ mol^{-1})$	$\Delta H^0_{ads}(kJ\ mol^{-1})$	$\Delta S^0_{ads}(J\ mol^{-1}K^{-1})$
298	-38.52766469		
308	-38.16614069		
318	-37.82372003	-31.68	23.5
328	-37.62285268		
338	-37.24511435		

Table 2 analysis shows that ΔG^0_{ads} values are negative and range between -20 $kJ\ mol^{-1}$ and -40 $kJ\ mol^{-1}$. In this case, according to the literature, the adsorption process is spontaneous, with the presence of two adsorption modes: chemical adsorption and physical adsorption [29,30]. ΔH^0_{ads} negative value indicates that adsorption of CBTM1HBI to aluminum surface is exothermic [31]. As for the positive value of ΔS^0_{ads}, it describes the increase in disorder during the adsorption process [32]. This increase in disorder causes water molecules to detach from the metal surface.

3.1.4. *Adsorption specificity*

Thermodynamic adsorption parameters interpretation reveals the presence of two adsorption modes. Adejo-Ekwenchi isotherm was used to distinguish the temperature ranges in which each type of adsorption occurs. The representation of this isotherm is given in Fig. 7, and its parameters are listed in Table 3. The equation of this adsorption isotherm is expressed as [33]:

$$log\left(\frac{1}{1-\theta}\right) = logK_{AE} + blogC_{inh} \quad (8)$$

K_{AE} and b are Adejo-Ekwenchi model parameters.

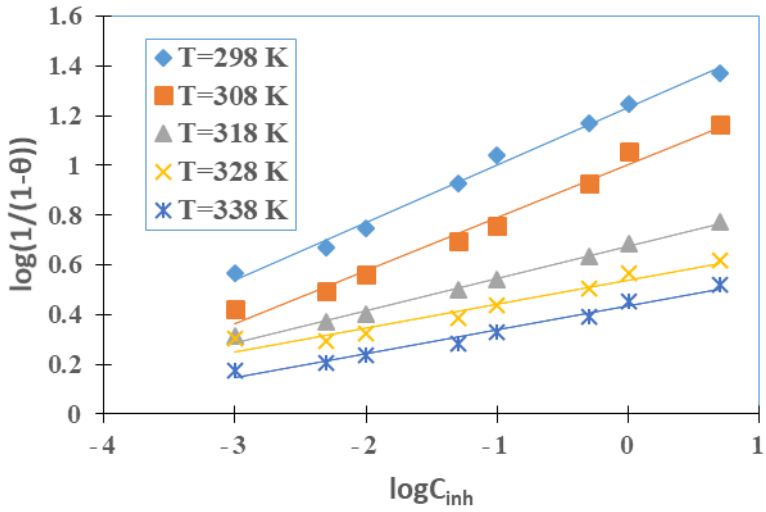

Fig. 7. Adejo–Ekwenchi adsorption model for CBTM1HBI adsorption.

Table 3. Adejo-Ekwenchi isotherm parameters.

T(K)	Equation	R^2
298	$log\left(\frac{1}{1-\theta}\right) = 0.2305 logC_{inh} + 1.2313$	0.9923
308	$log\left(\frac{1}{1-\theta}\right) = 0.2132 logC_{inh} + 1.0047$	0.9817
318	$log\left(\frac{1}{1-\theta}\right) = 0.1295 logC_{inh} + 0.6759$	0.993
328	$log\left(\frac{1}{1-\theta}\right) = 0.0961 logC_{inh} + 0.5387$	0.947
338	$log\left(\frac{1}{1-\theta}\right) = 0.0962 logC_{inh} + 0.4351$	0.9766

Table 3 shows that in temperature range from 298 K to 328 K, b parameter values decrease. These observations indicate that in this temperature range, CBTM1HBI adsorbs to aluminum in a physical way [33]. Which adsorption occurs via through electrostatic bonds between inhibitor protonated and NO_3^- ions. A protective layer resulting from these electrostatic interactions is formed on aluminum surface to reduce its dissolution. Whereas from 328 K to 338 K, parameter b values are constant [33]. It turns out that in this case CBTM1HBI establishes covalent bonds with the unfilled aluminum orbital.

3.1.5. *Activation parameters investigation*

Gravimetric tests revealed the influence of temperature on corrosion rate and inhibition efficiency. This influence permit to determine activation parameters from the following relationships [34]:

$$logW = logA - \frac{E_a}{2{,}3.R.T} \tag{9}$$

$$log(\frac{W}{T}) = log(\frac{R}{N_A.h}) + \frac{\Delta S_a^*}{2.3.R} - \frac{\Delta H_a^*}{2.3.R.T} \tag{10}$$

Where R is the universal gas constant, T is the absolute temperature, N_A is the Avogadro's number and h is the Planck's constant, activation energy (E_a), activation enthalpy (ΔH_a^*) and activation entropy (ΔS_a^*). The slopes of the straight lines in Fig. 7 are used to determine Ea. The slopes and intercepts of straight lines for Fig. 8 are used to determine activation enthalpy (ΔH_a^*) and entropy (ΔS_a^*) respectively. The valeurs of these activation parameters are listed in Table 4.

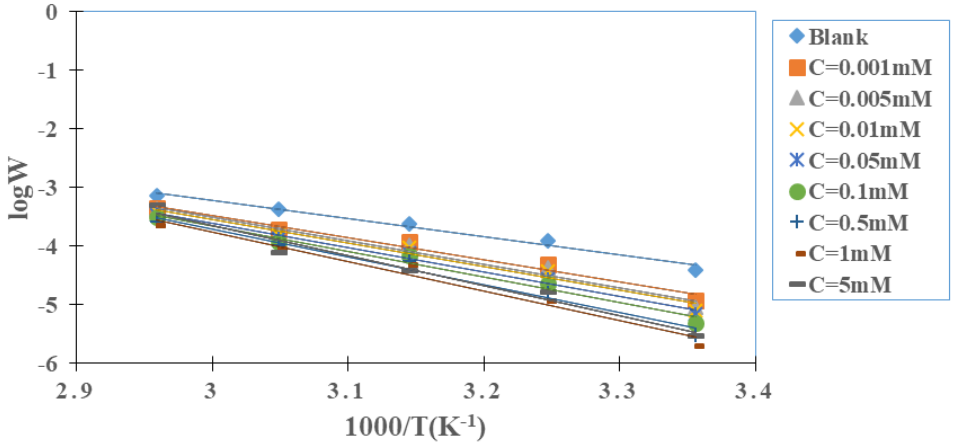

Fig. 7. Plots of log (*W*) versus 1/T.

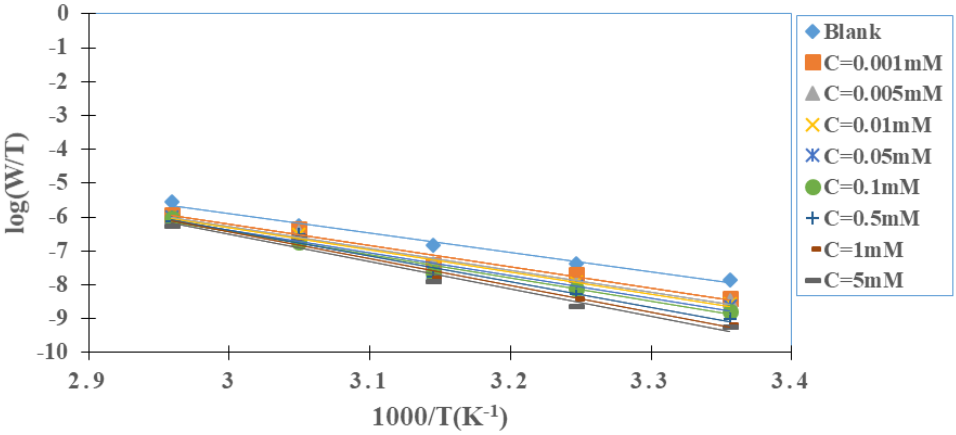

Fig. 8. Plots of log (*W*) versus 1/T.

Table 4. Valeurs des paramètres d'activation.

C_{inh} (mM)	$E_a(kJ.mol^{-1})$	$\Delta H_a^*(kJ.mol^{-1})$	$\Delta S_a^*(J.mol^{-1}.K^{-1})$
0	59.74004109	110.2828214	20.111936
0.001	72.14867878	120.7370412	45.54368
0.005	76.6457561	123.4904711	52.356096
0.01	77.43710374	125.7763736	58.537024
0.05	79.21332474	127.8553378	63.378432
0.1	83.49963149	132.1416445	75.510656
0.5	91.57214394	145.18451	115.313536
1	97.26294906	151.8678529	134.602624
5	98.85139264	153.3528273	137.339072

Table 4 shows that activation energy (E_a) values in solutions containing CBTM1HBI are higher than in the blank solution. These results indicate that aluminum dissolution is rapid in CBTM1HBI absence and difficult in its presence [35]. This dissolution becomes increasingly difficult as CBTM1HBI concentration increases. The enthalpy of activation (ΔH_a^*) values are positive and increase with inhibitor concentration. These values show that aluminum dissolution is endothermic and is reduced by CBTM1HBI presence. Moreover, the activation entropy (ΔS_a^*) values mentions that this dissolution is accompanied by an increase in disorder [35].

3.2. Analysis of theoretical findings

3.2.1. *Correlation between quantum chemical parameters and inhibition efficiency*

The quantum chemical parameters computed from DFT at B3LYP/6-311++(d,p) are : highest occupied molecular orbital energy (E_{HOMO}), lowest unoccupied molecular orbital energy (E_{LUMO}), energy gap (ΔE), dipole moment (μ), electron affinity (A), ionization energy (I), electronegativity (χ), hardness (η), softness (σ), electrophylicity index (ω),fraction of electron transferred (ΔN) and total energy (E_T). The values of these quantum chemical parameters are listed in Table 5.

The inhibition action of an organic compound on metal corrosion depends on its ability to exchange electrons with this metal. The reactivity parameters that influence these electronic exchanges are the highest occupied molecular orbital energy (E_{HOMO}) and lowest unoccupied molecular orbital energy. Indeed, a molecule with a high E_{HOMO} value is able to donate electrons to the metal [36]. On the other hand, when the molecule has a low E_{LUMO} value, it is more inclined to receive electrons from the metal [36]. 2-4-CBTM1HBI has a high E_{HOMO} value and a low E_{LUMO} value. In this case, it can both donate and receive electrons from aluminum. The inhibiting power of an organic compound also depends on the value of its energy gap (ΔE). Indeed, the lower the energy gap (ΔE), the more reactive the molecule, and consequently the higher its efficiency [37,38]. ΔE value obtained with 2-4-CBTM1HBI justifies the high inhibition efficiencies obtained experimentally. HOMO and LUMO energies show that electrons are exchanged between metal and inhibitor. Fig. 9 shows that the electronic distribution of HOMO and LUMO orbital densities are distributed over the benzene nuclei. This distribution shows that the interactions between metal and molecule are effectively dependent on HOMO and LUMO energies. The electronegativity value of the inhibitor (χ= 3.90 eV) is lower than that of aluminum (4.28eV), with $\Delta N > 0$. These results indicate that aluminum has more electron attraction capacity than the inhibitor. Consequently, electrons from the inhibitor move more towards the metal [39]. This massive movement of electrons towards the aluminum means that its electron loss to the corrosive medium is compensated. The corrosion rate of aluminum is thus reduced in 2-4-CBTM1HBI presence. These data confirm the good performance of 2-4-CBTM1HBI. The correlation between dipole moment (μ) and inhibition efficiency of a compound is the subject of much debate in the literature, with some authors arguing that a high value of μ

means that the molecule adsorbs more onto metal surface, while others believe that a low value of μ increases the inhibition power [40,41]. Dipole moment value obtained could justify the good adsorption capacity of inhibitor on metal surface. CBTM1HBI has a high softness value (σ) and a low hardness value (η). These different values certify that CBTM1HBI is unstable [42]. This instability is due to heteroatoms presence which are the adsorption sites. These adsorption sites establish covalent bonds with aluminum. The high value of the electrophilicity index (ω) expresses that CBTM1HBI can receive electrons from aluminum [43]. In fact, CBTM1HBI is protonated in the 1 M HNO_3 solution. This protonated form is more likely to receive electrons from aluminum to form a coordination bond on metal surface. CBTM1HBI's ability to donate and accept electrons is also justified by its low total energy value [44]. The electron donation and acceptance capability of CBTM1HBI is also justified by its low total energy value [45,46]. These electronic exchanges enhance the adsorption capacity of the inhibitor at the metal surface, thus justifying the gravimetric results.

Table 5. Quantum chemical parameters.

Quantum chemical parameters	Values	Quantum chemical parameters	Values
E_{HOMO} (eV)	-6.3376	$\chi = -\mu_p = \frac{I+A}{2}$ (eV)	3.7896
E_{LUMO} (eV)	-1.2417	$\eta = \frac{I-A}{2}$ (eV)	2.5479
$\Delta E = E_{LUMO} - E_{HOMO}$ (eV)	5.0959	$\sigma = \frac{1}{\eta}$ (eV)$^{-1}$	0.3924
μ (Debye)	4.2715	$\Delta N = \frac{\chi_{Al}-\chi_{inh}}{2(\eta_{Al}+\eta_{inh})}$	0.0962
$I = -E_{HOMO}$ (eV)	6.3376	$\omega = \frac{\mu_P^2}{2\eta} = \frac{(I+A)^2}{4(I-A)}$	2.8181
$A = -E_{LUMO}$ (eV)	1.2417	E_T (Ha)	-1547.5620

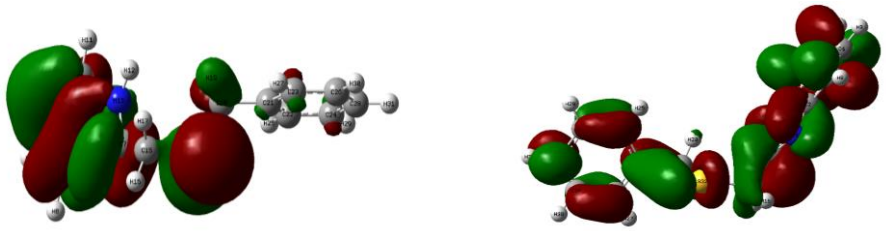

HOMO orbital LUMO orbital

Fig. 9. Electronic distribution of HOMO and LUMO orbital.

3.2.2. *Selectivity study*

Selectivity studies identify atoms within the molecule that are prone to electrophilic and nucleophilic attacks. Fukui functions and dual descriptors determined from Mulliken atomic charges are expressed as follows:

Nucleophilic attack $f_k^+ = q_k(N+1) - q_k(N)$ (11)

Electrophilic attack $f_k^- = q_k(N) - q_k(N-1)$ (12)

Dual descriptor $$\Delta f_k(\mathrm{r}) = f_k^+ - f_k^- \quad (12)$$

These values permit to select these reactivity sites [47,48]. Local reactivity parameter values are listed in Table 6. The probable site for nucleophilic attacks is the atom with the highest value of f_k^+ and $\Delta f_k(\mathrm{r})$.The atom with the highest value of f_k^- and the lowest value $\Delta f_k(\mathrm{r})$ is more prone to receive electrophilic attacks. In case of ambiguity, the dual descriptor can be used to validate the choice of reactivity site [49,50].

It emerges from Table 6 analysis that C(21) atom is the probable site for nucleophilic attacks and C(22) atom is the probable center for electrophilic attacks. These sites represent respectively the centers of electron loss and gain.

Table 6. Mulliken atomic charges, Fukui functions and the dual descriptor for CBTM1HBI by B3LYP / 6-31 G (d, p).

Atoms	$q_k(N+1)$	$q_k(N)$	$q_k(N-1)$	f_k^+	f_k^-	$\Delta f_k(\mathrm{r})$
C(1)	0.443	0.350	0.553	0.203	-0.093	0.296
C(2)	-0.009	0.442	0.251	-0.191	0.451	-0.642
C(3)	-0.384	-0.308	-0.222	0.086	0.076	0.010
C(4)	-0.335	-0.361	-0.364	-0.003	-0.026	0.023
C(5)	-0.376	-0.312	-0.248	0.064	0.064	0.000
C(6)	-0.484	-0.545	-0.523	0,022	-0.061	0.083
C(7)	0.396	0.105	-0.033	-0.138	-0.291	0.153
H(8)	0.150	0.181	0.228	0.047	0.031	0.016
H(9)	0.131	0.162	0.212	0.050	0.031	0.019
H(10)	0.145	0.164	0.224	0.060	0.019	0.041
H(11)	0.159	0.152	0.199	0.047	-0.007	0.054
H(12)	0.147	0.307	0.334	0.027	0.160	-0.133
N(13)	-0,101	0.003	0.096	0.093	0.104	-0.011
N(14)	0.097	-0.084	-0.045	0.039	-0.181	0.220
C(15)	-0.435	-0.790	-0.780	0,010	-0.355	0.365
H(16)	0.123	0.178	0.204	0.026	0.055	-0.029
H(17)	0.134	0.276	0.329	0.053	0.142	-0.089
C(18)	-0.592	-0.809	-1.305	-0.496	-0.217	-0.279
H(19)	0.132	0.156	0.257	0.101	0.024	0.077
H(20)	0.180	0.216	0.210	-0.006	0.036	-0.042
C(21)	1.150	0.697	1.152	**0.455**	-0.453	**0.908**
C(22)	-0.643	-0.056	-0.150	-0.094	**0.587**	**-0.681**
C(23)	-0.497	-0.447	-0.502	-0.055	0.050	-0.105
C(24)	-0.756	-0.847	-0.725	0.122	-0.091	0.213
H(25)	0.136	0,187	0.186	-0.001	0.051	-0.052
C(26)	-0.737	-0.865	-0.675	0.190	-0.128	0.318
H(27)	0.142	0.174	0.179	0.005	0.032	-0.027
C(28)	0.751	0.773	0.603	-0.170	0.022	-0.192
H(29)	0.165	0.188	0.221	0.033	0.023	0.010
H(30)	0.150	0.188	0.222	0.034	0.038	-0.004
S(31)	-0.734	0.107	0.378	0.271	0.841	-0.570
Cl(32)	0.342	0.420	0.532	0.112	0.078	0.034

3.3. *Inhibitor mechanism adsorption*

CBTM1HBI is protonated in HNO_3 1M according to the following equation:

$$CBTM1HBI + HNO_3 \rightleftarrows [CBTM1HBIH]^+ + NO_3^-$$

The protonated form $[CBTM1HBIH]^+$ will interact with NO_3^- and Al^{3+} on metal surface. A protective film resulting from the electrostatic interactions between these ions will form on aluminum surface. This film is sensitive to high temperatures. As a result, this film disappears less and less as the temperature rises. This explains the decrease in inhibition efficiency as temperature rises. After protonation, the electron capacity of the inhibitor decreases. The π-bonds and heteroatoms within the molecule then react with the vacant aluminum orbitals (3p) to form covalent bonds (chemical adsorption), allowing the molecule to adsorb onto metal surface. This adsorption occurs at high temperatures, after electrostatic bond reduction. Chemical bonds formation is due to molecule's descriptor parameters (E_{HOMO}, E_{LUMO}, ΔE and ΔN), which certify that the molecule can give and receive electrons from the metal. The layer formed from these chemical bonds becomes thinner as the temperature rises, justifying the low efficiency values at higher temperatures. This mechanism is illustrated in Fig. 10.

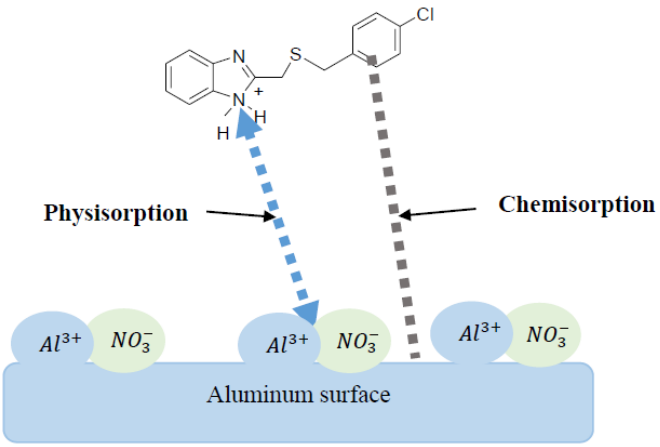

Fig. 10. CBTM1HBI Adsorption onto aluminium surface.

4. Conclusion

The inhibition performance of 2-(((4-chlorobenzyl) thiol) methyl)-1H-benzo[d]imidazole was studied. The gravimetric measurements used indicate that this compound has good anticorrosive performance. In fact, inhibition efficiency increases with inhibitor concentration and decreases with increasing temperature. These results expected the compound to be used at low temperatures. The adsorption mechanism is based on the Villamil adsorption model, with a combination of physical and chemical adsorption. The inhibitor adsorbs to the sample surface spontaneously, exothermically and accompanied by an increase in disorder. The study also revealed that aluminum dissolution in the solution

studied is slow in inhibitor presence. This dissolution is endothermic. Quantum chemical descriptors analysis revealed that the good inhibition performance of CBTM1HBI is based on its strong ability to exchange electrons with aluminum. The active centers within the inhibitor are carbons C(21) and C(22). DFT calculations and gravimetric results are in perfect agreement.

References

1. O. F. Akinyele , A. S. Adekunle, D. S. Olayanju, O. E. Oyeneyin, S. S. Durodola et al., J. Mol. Struct. **1268**, ID 133738 (2022). https://doi.org/10.1016/j.molstruc.2022.133738.
2. A. Al Bahir, Chem. Data Collect. **42**, ID 100960 (2022). https://doi.org/10.1016/j.cdc.2022.100960.
3. K. H. Rashid, A. A. Khadom, S. H. Abbas, K. F. Al-azawi, and H. B. Mahood, Res Surf. Interfaces **13**, ID 100165 (2023). https://doi.org/10.1016/j.rsurfi.2023.100165
4. M. Abdallah, H. Hawsawi, A. S. Al-Gorair, M. T. Alotaibi, S. S. Al-Juaid, and R. S. A. Hameed, Int. J. Electrochem. Sci. **17**, 220462 (2022). https://doi.org/10.20964/2022.04.61
5. E. Elqars, Y. Laamari, K. Sadik, A. Bimoussa, A. Oubella, et al., J. Mol. Struct. **1282**, ID 135228 (2023). https://doi.org/10.1016/j.molstruc.2023.135228
6. H. M. Abd El-Lateef, Z. A. Abdallah, and M. S. M. Ahmed, J. Mol. Struct. **296**, ID 111800 (2019). https://doi.org/10.1016/j.molliq.2019.111800.
7. H. M. Abd El-Lateef, M. A. Abo-Riya, and A. H. Tantawy, Corros. Sci. **108**, 94 (2016). https://doi.org/10.1016/j.corsci.2016.03.004.
8. P. Vashishth , B. Mangla, H. Bairagi, R.Narang, and S. K Shukla, Chem. Eng. Commun. **211**, 526 (2024). https://doi.org/10.1080/00986445.2023.2255545
9. V. Priya, H. Bairagi, R. Narang, S. K. Shukla, and M. Bindu, J. Mol. Liq. **365**, ID 120042 (2022). https://doi.org/10.1016/j.molliq.2022.120042
10. P. Vashishth, H. Bairagi, R. Narang, S. K. Shukla, L. O. Olasunkanmi, and E. E. Ebenso, Res. Surf. Interfaces **13**, ID 100155 (2023). https://doi.org/10.1016/j.rsurfi.2023.100155
11. R. Lei, S. Deng, Y. Qiang, D. Xu, G. Du, D. Shao, and X. Li, Colloids Surf. A **687**, ID 133358 (2024). https://doi.org/10.1016/j.colsurfa.2024.133358
12. E. D. Akpan, A. K. Singh, H. Lgaz, T. W. Quadri, and S. K. Shukla, Coord. Chem. Rev. **499**, ID 215503 (2024). https://doi.org/10.1016/j.ccr.2023.215503.
13. T. Chen, H. Gan, Z. Chen, and M. Chen, J. Mol. Struct. **1244**, ID 130881 (2021). https://doi.org/10.1016/j.molstruc.2021.130881
14. S. Bashir, A. Thakur, H. Lgaz, Ill-Min Chung, and A. Kumar, Surf. Interfaces **20**, ID 100542 (2020). https://doi.org/10.1016/j.surfin.2020.100542.
15. S. M. Syam, E. E. El-Katori, A.. A. Elhenawy, H. Nady, and S. Eid, RSC Adv. **16**, ID 11244 (2024). https://doi.org/10.1039/d4ra00158c
16. R. Padash, G. S. Sajadi, A. H. Jafari, E. Jamalizadeh, and A. S. Rad, Mater. Chem. Phys. **244**, ID 122681 (2020). https://doi.org/10.1016/j.matchemphys.2020.122681
17. W. Nawrocka, B. Sztuba, M. W Kowalska, H. Liszkiewicz, J. Wietrzyk, A. Nasulewicz, M. Pełczyńska, and A. Opolski, Il Farmaco **59**, 83 (2004). https://doi.org/10.1016/j.farmac.2003.12.001
18. M. J. Frisch, G. W. Trucks, H. B. Schlegel, G. E. Scuseria, M. A. Robb et al., Gaussian 03, Revision B.05, Gaussian, Inc., Pittsburgh PA (2003).
19. C. Lee, W. Yang, and R. G. Parr, Phys. Rev. B **37**, 785 (1988).
20. L. Gao, S. Peng, X. Huang, and Z. Gong, Appl. Surf. Sci. **511**, ID 145446 (2020). https://doi.org/10.1016/j.apsusc.2020.145446
21. M. Tang, S. Deng, J. Xu, D. Xu, D. Shao, and G. Du, X. Li, Corros. Sci. **228**, ID 111799 (2024). https://doi.org/10.1016/j.corsci.2023.111799.
22. R. Lei, S. Deng, Y. Qiang, D. Xu, G. Du, D. Shao, and X. Li, Colloids Surf. A **687**, ID 133358 (2024). https://doi.org/10.1016/j.colsurfa.2024.133358

23. D. I. Njoku, I. Ukaga, O. B. Ikenna, E. E. Oguzie, K. L. Oguzie, J. Mol. Struct. **219**, 417 (2016). https://doi.org/10.1016/j.molliq.2016.03.049
24. M. Abdallah, M. Sobhi, and H. M. Altass, J. Mol. Struct. **223**, 1143 (2016). https://doi.org/10.1016/j.molliq.2016.09.006
25. `K. Zhang, W. Yang, Bin Xu, Y. Chen, X. Yin, Ying Liu, and H. Zuo , J. Colloid Interface Sci. **517**, 52 (2018). https://doi.org/10.1016/j.jcis.2018.01.092
26. I. Langmuir, J. Am. Chem. Soc. **38**, 2221 (1916). https://doi.org/10.1021/ja02268a002
27. R. F. Villamil, V. Corio, P. J. C. Rubin, and S. M. L. Agostinho. J. Electroanal. Chem. **472**, 112 (1999). https://doi. org/10.1016/S0022-0728 (99)00267-3
28. Mustapha, R. Oukhrib, Y. A. Albrimi, H. A. Oualid, H. Bourzi, R. A. Akbour, A. Assabbane, A. Nahle, and M. Hamdani, RSC Adv. **10**, 41137 (2020). https://doi.org.10.1039/d0ra06742
29. M. Solomon, S. A. Umoren, M.A. Quraishi, and M. Salman, J. Colloid Interface Sci. **551**, 47 (2019). https://doi.org/10.1016/j.jcis.2019.05.004
30. A. Dehghani, G. Bahlakeh, B. Ramezanzadeh, and M. Ramezanzadeh, J. Mol. Struct. **279**, 603 (2019). https://doi.org/10.1016/j.molliq.2019.02.010
31. Y. M. Behera D, U. Sharma, Arabian J. Chem. **9**, S1487 (2016). https://doi.org/10.1016/j.arabjc.2012.03.011
32. V. R. Saliyan and A.V. Adhikari. Bull. Mater. Sci. **31**, 699 (2008). https://doi.org/10.1007/s12034-008-0111-4
33. S. O. Adejo and M. M. Ekwenchi, J. Emerging Trends Eng. Appl. Sci. **5**, 201 (2014).
34. M. E. Faydy, M. Rbaa, L. Lakhrissi, B. Lakhrissi, I. Warad, A. Zarrouk, and I. B. Obot, Surf. Interfaces **14,** 222 (2019). https://doi.org/10.1016/j.surfin.2019.01.005
35. R. H. B. Beda , M. A. Tigori, D. Diabaté, and P. M. Niamien, Curr. Phys. Chem. **11**, 227 (2021). https://doi.org/10.2174/1877946811666210526152314
36. D. I. Udunwa, O. D. Onukwuli, S. C. Nwanonenyi, and C. B. Ezekannagha, Appl. Surf. Sci. Adv. **19**, ID 100578 (2014). https://doi.org/10.1016/j.apsadv.2024.100578
37. B. Tan, S. Zhang, H. Liu, Y. Guo, Y. Qiang, W. Li, L. Guo, C. Xu, and S. Chen, J. Colloid Interface Sci. **538**, 519 (2019). https://doi.org/10.1016/j.jcis.2018.12.020
38. P. Han, C. Chen, W. Li, H. Yu, Y. Xu, L. Ma, and Y. Zheng, J. Colloid Interface Sci. **516**, 398 (2018). https://doi.org/10.1016/j.jcis.2018.01.088
39. J. Zhang, W. Li, X. Zuo, Y. Chen, W. Luo, Y. Zhang, A. Fu, B. Tan, and S. Zhang, J. Taiwan Inst. Chem. Eng. **122**, 190 (2021). https://doi.org/10.1016/j.jtice.2021.04.035
40. L. Zhou, S. Zhang, B. Tan, L. Feng, B. Xiang, F. Chen, W. Li, and B. Xiong, J. Taiwan Inst. Chem. Eng. **113**, 253 (2020). https://doi.org/10.1016/j.jtice.2020.08.018
41. N. A. Wazzan, I. B. Obot, and S. Kaya, J. Mol. Struct. **221**, 579 (2016), https://doi.org/10.1016/j.molliq.2016.06.011.
42. S. Vandana , Y. Mahendra, I. B. Obot, and I. B. Colloids Surf. A **599**, ID 124881 (2020). https://doi.org/10.1016/j.colsurfa.2020.124881.
43. R. G. Parr, L. Sventpaly, and S. Liu, J. Am. Chem. Soc. **121**, 1922 (1999). https://doi.org/10.1021/ja983494x
44. B. G. Prakashaiah, D. V. Kumara, A. A. Pandith, A. N. Shetty, and B. E. A. Rani, Corros. Sci. **136**, 326 (2018). https://doi.org/10.1016/j.corsci.2018.03.021
45. Y. Boughoues, M. Benamira, L. Messaadia, and N. Ribouh, Colloids Surf. A **593**, ID 124610 (2020). https://doi.org/10.1016/j.colsurfa.2020.124610
46. D. I. Udunwa, O. D. Onukwuli, M. C. Menkiti, S. C. Nwanonenyi, C. B. Ezekannagha, and C. O. Aniagor, J. Mol. Struct. **1302**, ID 137508 (2024). https://doi.org/10.1016/j.molstruc.2024.137508
47. S. Pareek, D. Jain, S. Hussain, A. Biswas, R. Shrivastava, S. K. Parida, H. K. Kisan, H. Lgaz, Ill-Min Chung, and D. Behera, Chem. Eng. J. **358**, 725(2019) https://doi.org/10.1016/j.cej.2018.08.079
48. A. Singh, K.R. Ansari, A. Kumar, W. Liu, C. Songsong, and Y. Lin, J. Alloys Compd. **712**, 121 (2017). https://doi.org/10.1016/j.jallcom.2017.04.072

49. C. Morell, A.Grand, and A.Toro-Labbé, J. Phys. Chem. A, **109**, 205 (2005). https://doi.org/10.1021/jp046577a
50. J. I. Martínez-Araya, J. Math. Chem. **5**, 451 (2015). https://doi.org/10.1007/s10910-014-0437-7